



CHORUS

This is the accepted manuscript made available via CHORUS. The article has been published as:

Using Disorder to Overcome Disorder: A Mechanism for Frequency and Phase Synchronization of Diode Laser Arrays

N. Nair, K. Hu, M. Berrill, K. Wiesenfeld, and Y. Braiman

Phys. Rev. Lett. **127**, 173901 — Published 22 October 2021

DOI: [10.1103/PhysRevLett.127.173901](https://doi.org/10.1103/PhysRevLett.127.173901)

Disorder + Disorder = Order; Cavity Misalignment Disorder Induces Frequency and Subsequently Phase-Locking of Semiconductor Diode Laser Arrays

N. Nair⁽¹⁾, K. Hu⁽¹⁾, M. Berrill⁽²⁾, K. Wiesenfeld⁽³⁾, and Y. Braiman^{(1,4)*}

⁽¹⁾ The College of Optics and Photonics (CREOL), University of Central Florida, Orlando, FL 32816

⁽²⁾ Computer Science and Mathematics Division, Oak Ridge National Laboratory, Oak Ridge, TN 37831

⁽³⁾ School of Physics, Georgia Institute of Technology, Atlanta, GA 30332

⁽⁴⁾ Department of Electrical and Computer Engineering, University of Central Florida, Orlando, FL 32816

Abstract: Noise and disorder are known, in certain circumstances and for certain systems, to improve the level of coherence over that of the noise-free system. Examples include cases in which disorder enhances response to periodic signals, and those where it suppresses chaotic behavior. We report a new type of disorder-enhancing mechanism, observed in a model that describes the dynamics of external cavity-coupled semiconductor laser arrays, where disorder of one type mitigates (and overcomes) the desynchronization effects due to a different disorder source. Here we demonstrate stabilization of dynamical states due to frequency locking and subsequently frequency locking-induced phase locking. We have reduced the equations to a phase model that illustrates the mechanism behind the misalignment-induced frequency and phase synchronization.

Synchronization in networks of nonlinear elements, including semiconductor diodes, has been studied, revealing a variety of spatial and temporal behaviors [1-22]. The equations describing the dynamics of a semiconductor diodes and diode arrays have been experimentally verified and extensively tested [3, 23-29]. Nearest neighbor coupled semiconductor lasers can be phase synchronized [24-26]; however, for large arrays, the in-phase solution destabilizes, and spatiotemporal chaos may occur. This destabilization occurs because as coupling strength increases, the number of external cavity modes increases and the coupled lasers chaotically hop between these fixed-frequency solutions [3, 27, 29].

Although noise and/or spatial disorder typically are expected to reduce coherent behavior, under certain circumstances they can improve it [30-45]. In one widely studied class, known as stochastic resonance, dynamical noise enables the influence of a weak periodic force [30,31]. It has been recently suggested that uncorrelated noise can promote rather than inhibit coherence in natural systems and that the same effect can be harnessed in engineered systems [32]. Alternatively, quenched disorder can suppress or eliminate large deterministic fluctuations of a chaotic system to yield synchronized behavior [33-41]. Coupled dynamical systems with highly heterogeneous time delays or other system parameters have been studied [22,46-48].

In this paper, we identify a new mechanism in single-mode semiconductor lasers whereby the addition of disorder enhances system-wide coherence. We find that one type of disorder mitigates array desynchronization shaped by a different type of

disorder and generates a highly ordered dynamical state. While the nature of disorder-enhanced synchronized states could vary both temporally (i.e., fixed point solutions, limit cycles, quasiperiodic solutions, etc.) and spatially (external cavity modes, in-phase solutions, etc.), we focus our attention on states that lead to the high degree of frequency and phase-locking important for a variety of applications. We demonstrate a disorder-driven mechanism by which frequency and frequency-induced phase-locking is achieved.

We begin with a version of the Lang-Kobayashi (LK) equations that has gain saturation nonlinearity and amplitude-phase coupling. We describe the i th laser field $E_i(t) = r_i(t)e^{i\phi_i(t)}$ and carrier number $N_i(t)$ in an array of M lasers [49-54]:

$$\begin{aligned}\dot{E}_i(t) &= \frac{1+i\alpha}{2} \left(g \frac{N_i(t) - N_0}{1+s|E_i(t)|^2} - \gamma \right) E_i(t) + i\sigma\omega_i E_i(t) + \frac{\kappa^f}{M} \sum_{j=1}^M K_{ij} E_j(t - \tau + \varepsilon\tau_{ij}) + F_{E_i} \\ \dot{N}_i(t) &= J_0 - \gamma_n N_i(t) - g \frac{N_i(t) - N_0}{1+s|E_i(t)|^2} + F_{N_i}\end{aligned}\quad (1)$$

Here, $N_0 = 1.5 \times 10^8$ is the number of carriers at transparency, $g = 1.5 \times 10^{-8} \text{ ps}^{-1}$ and $s = 2 \times 10^{-7}$ are the differential gain coefficient and the gain saturation coefficient respectively [50,51], $\gamma = 0.5 \text{ ps}^{-1}$ is the cavity loss, $\alpha = 5$ is the linewidth enhancement factor [52,53], $\gamma_n = 0.5 \text{ ns}^{-1}$ is the carrier loss rate, $J_0 = a\gamma_n(N_0 - \frac{\gamma}{g})$ is the pump current, κ^f is the feedback strength, F_E are complex Gaussian noise, $\langle F_{E_i}(t), F_{E_j}^*(t') \rangle = R_{sp} \delta_{ij} \delta(t-t')$, and F_N are real Gaussian noises, $\langle F_{N_i}(t), F_{N_j}(t') \rangle = \gamma_n N_i(t) \delta_{ij} \delta(t-t')$ [54,55]. The frequency detuning of the i th laser is $\sigma\omega_i$ where ω_i is a random fixed real number distributed with zero mean and 2π variance, and σ represents the variance of the detuning with units ns^{-1} . For simulations, we use a fourth order Adams-Bashforth-Moulton stochastic integration method [56]. We note that the effects discussed in this paper occur without noise, however we include the noise term to illustrate that the phenomenon is robust.

The delay time between the i and j lasers has an offset $\varepsilon\tau_{ij} = \varepsilon(\eta_i + \eta_j)$, the vector $\boldsymbol{\eta}$ is a random vector of time-delays drawn from a positive half-normal distribution with zero mode, variance $(1 - \frac{2}{\pi})$, $\varepsilon\eta_i$ and $\varepsilon\eta_j$ are positive (and hence τ_{ij} is positive). The value of time delay ($\tau = 3 \text{ ns}$) is large enough not to consider multiple reflections from the misaligned facets [57, 58]. The parameter ε is related to the variance of the delay misalignment and has units of ns. Here, we note that typically a phase factor proportional to the time-delay and carrier frequency $e^{i\omega_0\varepsilon\tau_{ij}}$ multiplies the feedback term. For a typical diode laser, the period is $\frac{2\pi}{\omega_0} \sim 10^{-6} \text{ ns}$, whereas the misalignment of the i th laser is $\varepsilon\eta_i \sim 10^{-1} \text{ ns}$, consequently, the misalignment parameters can be slightly adjusted by less than a

wavelength to negate the phase-shift without significantly changing the delay time misalignment. Therefore, we assume that $\varepsilon\eta_i$ is an integer multiple of $\frac{2\pi}{\omega_0}$. We note that

disorder does not have to be random: engineered or random engineered disorder can lead to very similar outcomes promoting synchrony in the system. We therefore do not include the phase factor. We have numerically confirmed in several examples that adding $e^{i\omega_0\varepsilon\tau_{ij}}$ to the feedback term does not change the main results of our paper and will only make the mathematical description of the underlying mechanism more complicated.

We consider the decayed nonlocal coupling matrix \mathbf{K} whose ij element is $K_{ij} = d_x^{i-j}$ where $d_x \in (0,1)$. In the case of a 2-dimensional array, the matrix element coupling the ik laser with the jl laser is $K_{ij,kl} = d_x^{i-j} d_y^{k-l}$, where $d_x, d_y \in (0,1)$. This matrix corresponds in principle to many external cavity designs because the mode structure is similar to that of a resonator with "good" properties [14,21,59,60].

In an array of identical lasers ($\sigma = 0$) coupled with decayed nonlocal coupling \mathbf{K} and no misalignment ($\varepsilon = 0$), phase locking occurs as a form of array-wide transverse mode selection, where the dynamics of the mode selected by the array are similar to the dynamics of a single laser with an effective feedback constant $\kappa' = \frac{\kappa^f}{M} \lambda_1$ where λ_1

is the largest eigenvalue of \mathbf{K} [61,62]. This phase locked state is robust to small amounts of frequency detuning and the phase-locking persists even in chaotic parameter ranges [61]. However, when detuning becomes too large, the lasers begin to desynchronize. If a laser in the array has a frequency ω_i that is far from the central

frequency $\frac{1}{M} \sum_j \omega_j$, then it becomes unlikely for the laser to participate in the phase-locked state.

Even when natural frequencies of individual lasers are far enough apart to cause desynchronization, we find that introduction of facet misalignment causes all lasers to converge perfectly to a single frequency. In Figure 1 we show $\cos(\phi_i)$ for a 10x10 diode laser array without and with facet misalignment, and corresponding power spectra. We have tested different size arrays, 1-dimensional and 2-dimensional, and confirmed that the results in Figure 1 are typical for different sizes and parameters.

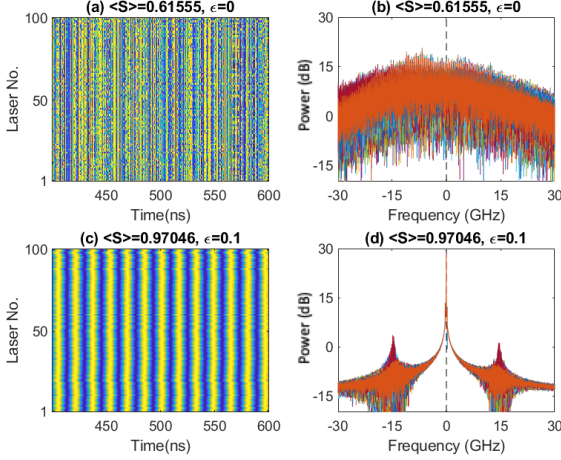


Figure 1: (a, c) $\cos\phi_i$ (blue is -1 and yellow is +1) as a function of time (x-axis) and laser number (y-axis) for a two-dimensional array of $M = 100$ lasers with $d_x = d_y = 0.95$ and $\kappa^f = 30ns^{-1}$. (b, d) The corresponding power spectra. The lasers are detuned with variance of $\sigma = 3GHz$. For the top figures, the facets are perfectly aligned $\varepsilon = 0$, and for the bottom figures, the facet is misaligned so that $\varepsilon = 0.1$.

We observe that with $\varepsilon = 0$ the power spectrum of all lasers is broad, indicating chaotic behavior. Further, detuning is large enough that average phase

synchronization $\langle S \rangle = \left\langle \frac{|\sum_{i=1}^M E_i(t)|^2}{M \sum_{i=1}^M |E_i(t)|^2} \right\rangle$ is low. With facet misalignment, phase

synchronization improves to almost perfect phase synchrony and all lasers lock to a single frequency. We have tested disorder-enhanced frequency-locking for 100 different misalignment disorder realizations and random-phase, zero-amplitude initial conditions and find very similar results.

It is well-known that for a single laser, the Lang-Kobayashi equations' solution-space is determined by the stability properties of the External Cavity Mode (ECM) solutions [63-68]. Each solution is a fixed-frequency fixed-intensity solution. As feedback strength to a laser is increased, the number of ECMs increases [64]. It has been shown [61,62] that coupled array (without misalignments) can synchronize on a collective mode and undergo the same feedback-induced bifurcation cascade as a single laser. For weak to moderate feedback, this synchrony is stable. However, for sufficiently large feedback strength that is required to phase-locking moderately frequency-detuned arrays, the chaotic behavior destabilizes synchrony [61,62]. In this strong feedback regime, "attractor hopping" takes place where the frequencies of the individual lasers slowly hop between the ECM frequencies [61,62,64,69,70]. The power spectrum for $\varepsilon = 0$ in Figure 1(b) indicates chaotic behavior with many frequencies, in contrast to a single dominant frequency for $\varepsilon \neq 0$ seen in Figure 1(d). The presence of misalignment destabilizes all but a single fundamental frequency for the system, even though each laser has a detuned central frequency.

We begin by changing Equation (1) to polar coordinates such that $E_i(t) = r_i(t)e^{i\phi_i(t)}$ and use $G(N_i, r_i) = (g \frac{N_i - N_0}{1 + sr_i^2} - \gamma)$. Since J_0 is much higher than threshold, all the ECM

solutions that we consider are within the gain bandwidth for the system, so we will not need to use the carrier number equation for this analysis. We now consider dynamics on the timescale of the ECM frequencies. In diode lasers ECM frequencies are much lower than relaxation oscillation frequencies [64,69-71]. Therefore, in our derivation the effects of carrier dynamics will be effectively treated as fluctuations about ECM solutions. We also assume constant (or fluctuating around constant) value for field amplitudes r_i . These assumptions are further justified in the Supplement S1. Equations (1) reduce to:

$$0 = \frac{1}{2}G + \frac{\kappa^f}{M} \sum_j K_{ij} \cos(\phi_j(t - \tau + \varepsilon\tau_{ij}) - \phi_i) + \frac{1}{r} \Re(F_{E_i} e^{-i\phi_i})$$

$$\dot{\phi}_i = \frac{\alpha}{2}G + \sigma\omega_i + \frac{\kappa^f}{M} \sum_j K_{ij} \sin(\phi_j(t - \tau + \varepsilon\tau_{ij}) - \phi_i) + \frac{1}{r} \Im(F_{E_i} e^{-i\phi_i})$$
(2)

Combining these, we arrive at a time-delayed phase equation with added noise similar to that in [73]:

$$\dot{\phi}_i = \sigma\omega_i + \frac{\kappa^f}{M} \sqrt{1 + \alpha^2} \sum_j K_{ij} \sin(\phi_j(t - \tau + \varepsilon\tau_{ij}) - \phi_i - \tan^{-1}(\alpha))$$

$$- \frac{\sqrt{1 + \alpha^2}}{r} |F_{E_i}| \sin(\arg(F_{E_i}) - \phi_i - \tan^{-1}(\alpha))$$
(3)

We simplify the noise term as:

$$- \frac{\sqrt{1 + \alpha^2}}{r} |F_{E_i}| \sin(\arg(F_{E_i})) \rightarrow \frac{\sqrt{1 + \alpha^2}}{r} F_{\phi_i}$$

where F_{ϕ_i} is real Gaussian white noise: $\langle F_{\phi_i}(t), F_{\phi_j}(t') \rangle = \frac{R_{sp}}{2} \delta_{ij} \delta(t - t')$. We then rewrite Equation (3) as:

$$\dot{\phi}_i = \sigma\omega_i + \frac{\kappa^f}{M} \sqrt{1 + \alpha^2} \sum_j K_{ij} \sin(\phi_j(t - \tau + \varepsilon\tau_{ij}) - \phi_i - \tan^{-1}(\alpha)) + \frac{\sqrt{1 + \alpha^2}}{r} F_{\phi_i}$$
(4)

We can now consider fluctuations of the central frequency of each laser, rather than the phase. This treatment is similar to that in [69,72]. We assume, as in the simulation, that the individual laser frequencies vary on a time scale longer than τ . Then the frequency of i th laser can be approximated by $\Omega_i(t) \approx (\phi_i(t) - \phi_i(t - \tau)) / \tau$ and the evolution of Ω_i can be written as $\dot{\Omega}_i = (\dot{\phi}_i(t) - \dot{\phi}_i(t - \tau)) / \tau$:

$$\dot{\Omega}_i = \frac{\sigma\omega_i}{\tau} + \frac{\kappa^f}{M\tau} \sqrt{1 + \alpha^2} \sum_j K_{ij} \sin(\phi_j(t - \tau + \varepsilon\tau_{ij}) - \phi_i - \tan^{-1}(\alpha))$$

$$+ \frac{\sqrt{1 + \alpha^2}}{r} \frac{F_{\phi_i}}{\tau} - \frac{\dot{\phi}_i(t - \tau)}{\tau}$$
(5)

The time scale of variation of the frequency Ω_i is much larger than τ . We then approximate the instantaneous frequency $\dot{\phi}_i(t-\tau)$, assuming it resides on a single frequency during a delay interval (which is substantiated by our numerical experiments in this parameter range) [72]:

$$\dot{\phi}_i(t-\tau) \approx \frac{\phi_i(t) - \phi_i(t-\tau)}{\tau} + \frac{\sqrt{1+\alpha^2}}{r} F_{\phi_i}(t-\tau) = \Omega_i + \frac{\sqrt{1+\alpha^2}}{r} F_{\phi_i}(t-\tau) \quad (6)$$

According to the simulations presented here and the results of [61,62], the steady state solutions of the array in the case of small σ and $\varepsilon = 0$ are similar to the ECM solutions for a single laser, which satisfy $\Omega = \omega + \kappa^f \sqrt{1+\alpha^2} \sin(-\Omega\tau - \arctan(\alpha))$. For an array of lasers, the array solutions are similarly ECM solutions of a single laser with a modified effective coupling [61,62]. We therefore approximate the feedback term in the case of $\varepsilon = 0$ using $\sin(\phi_j(t-\tau) - \phi_i(t) - \tan^{-1}(\alpha)) \approx \sin(-\Omega_j\tau - \tan^{-1}(\alpha))$:

$$\begin{aligned} & \sin(\phi_j(t-\tau + \varepsilon\tau_{ij}) - \phi_i(t) - \tan^{-1}(\alpha)) \\ & \approx \sin(\phi_j^\tau - \phi_i - \tan^{-1}(\alpha)) + \varepsilon\tau_{ij}\dot{\phi}_j^\tau \cos(\phi_j^\tau - \phi_i - \tan^{-1}(\alpha)) \end{aligned} \quad (7)$$

$$\begin{aligned} & \sin(\phi_j^\tau - \phi_i - \tan^{-1}(\alpha)) + \varepsilon\tau_{ij}\dot{\phi}_j^\tau \cos(\phi_j^\tau - \phi_i - \tan^{-1}(\alpha)) \\ & \approx \sin(-\Omega_j\tau - \tan^{-1}(\alpha)) + \varepsilon\tau_{ij}(\Omega_j - \Omega_i) \end{aligned} \quad (8)$$

The first approximation in (7) is simply a first-order expansion. We make the stronger approximation (8) as an ansatz. This stronger approximation seems to work for the set of parameters and system considered in this paper and has been numerically verified (see Supplement S2).

We then arrive at the expression:

$$\begin{aligned} \dot{\Omega}_i &= \frac{1}{\tau}(\sigma\omega_i - \Omega_i) \\ &+ \kappa^f \frac{\sqrt{1+\alpha^2}}{M\tau} \sum_{j=1}^M K_{ij} \sin(-\Omega_j\tau - \tan^{-1}(\alpha)) + \varepsilon\kappa^f \frac{\sqrt{1+\alpha^2}}{M\tau} \sum_{j=1}^M K_{ij}\tau_{ij}(\Omega_j - \Omega_i) \\ &+ \frac{\sqrt{1+\alpha^2}}{r} \frac{F_{\phi_i}(t) - F_{\phi_i}(t-\tau)}{\tau} \end{aligned} \quad (9)$$

Since the noise sources $F_{\phi_i}(t)$ and $F_{\phi_i}(t-\tau)$ are uncorrelated, we can replace their sum with $F_{\Omega_i}(t)$ having magnified diffusion coefficient $2R_{sp} \frac{\sqrt{1+\alpha^2}}{r}$ (which is four times that of F_{ϕ_i}) [72]. The fully reduced system is:

$$\dot{\Omega}_i = \frac{1}{\tau}(\sigma\omega_i - \Omega_i) + \kappa^f \frac{\sqrt{1+\alpha^2}}{M\tau} \sum_j K_{ij} (\sin(-\Omega_j\tau - \tan^{-1}(\alpha)) + \varepsilon\tau_{ij}(\Omega_j - \Omega_i)) + F_{\Omega_i}(t) \quad (10)$$

When $\varepsilon = 0$, the Ω_i are essentially uncoupled. This does not imply that the actual laser dynamics is uncoupled. For $\varepsilon = 0$ the only frequency-locking mechanism could be related to the coupling matrix term $\sum_j K_{ij}$ that would be almost equal for large arrays. This coupling term may be too small to overcome the random detuning, leading to poor frequency - and thus phase-locking. Equation 10 shows that misalignment affects coupling and as demonstrated in Figure 1, can induce frequency locking.

To gain further insight into this mechanism, we recast Equation 10 as a potential system:

$$\begin{aligned} \dot{\Omega}_i &= -\frac{\partial V(\vec{\Omega})}{\partial \Omega_i} + F_{\Omega_i}(t) \\ V(\vec{\Omega}) &= -\frac{1}{2\tau} \sum_{i=1}^M (\sigma\omega_i - \Omega_i)^2 - \kappa^f \frac{\sqrt{1+\alpha^2}}{M\tau^2} \sum_{i=1}^M \sum_{j=1}^M K_{ij} \cos(\Omega_i\tau + \tan^{-1}\alpha) \\ &\quad - \varepsilon \frac{\kappa^f \sqrt{1+\alpha^2}}{4M\tau} \sum_{i=1}^M \sum_{j=1}^M K_{ij} \tau_{ij} (\Omega_j - \Omega_i)^2 \end{aligned} \quad (11)$$

There are three components to the potential function (see Figure 2). The first term, which includes the detuning, leads to a parabolic potential with a minimum (for an individual laser) at $\sigma\omega_i$ so that the potential minima of two detuned lasers are pulled apart, as illustrated in Figure 2(a). The second term of the potential can be thought of as an ECM contribution. The increase in the number of ECM solutions increases the number of local minima. The third term, proportional to ε , generates a "spring-like force" (Figure 2(b)): misalignment ($\varepsilon \neq 0$) effectively forces the frequencies of lasers towards one another. The presence of sufficiently large κ^f makes it possible for two lasers' delay coordinates to settle into local minima that have nearly equal frequency; however, it is nonzero ε that induces exact frequency alignment.

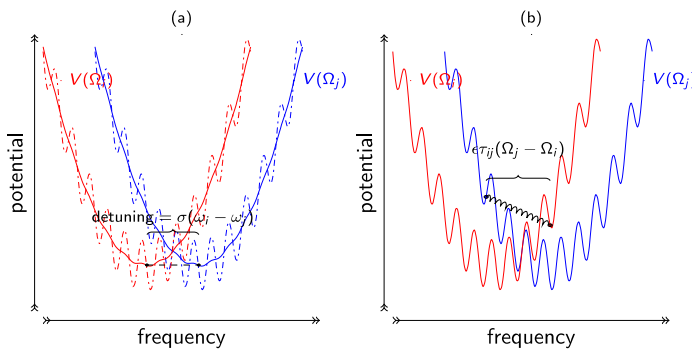


Figure 2: Diagrams of the effective potential functions of two detuned lasers' delay coordinates for $\varepsilon = 0$ (a) and $\varepsilon \neq 0$ (b). The solid lines denote the potentials for a very small value of κ^f and the dash-dotted lines denote the potentials for increased κ^f .

We illustrate the behavior of the potential model (Eq. (11)) in Figure 3 (left panel), where approximate steady-state values of Ω_i are plotted as a function of ε . The data is from a single simulation that starts with $\varepsilon = 0$, increasing ε by 0.001 ns every 400 time units. It is clear from the figure that as ε increases, the frequencies of the lasers are pulled together. Further, there are clearly discrete frequencies to which the Ω_i converge. To test that misalignment in the form of nonzero ε is the fundamental cause of frequency locking, we use the full system of equations (Eq. (1)) and follow a similar procedure to the one shown in the left panel of Figure 3. We consider a system of 10 lasers that are initially perfectly aligned. In a continuous simulation, every 300ns the misalignment scaling ε is increased by 0.001 ns. We record the delay coordinate for each laser (which should be related to the main frequency of the laser) at the last 30ns of each time segment and plot the set of points as a function of ε (Figure 3, right panel). The arrays have the same instance of frequency disorder with $\sigma = 3\text{GHz}$.

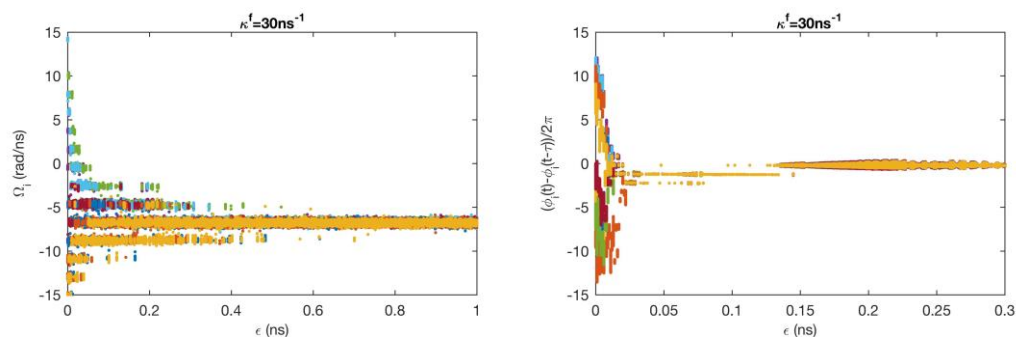


Figure 3: (left panel), values of Ω_i are plotted for each laser for a potential model (Eq. (11)) simulation of an array of 10 detuned lasers ($\sigma = 3\text{GHz}$) with $d_x = 0.8$. (right panel), phase delay $(\phi_i(t) - \phi_i(t - \tau)) / 2\pi$ is plotted for each laser in an array of 10 lasers. This plot is generated from a single simulation with 10 detuned lasers ($\sigma = 3\text{GHz}$) with $d_x = 0.8$ and slowly increasing ε . The same realizations of τ_{ij} and ω_i are used for each simulation. The coupling strength is $\kappa^f = 30\text{ns}^{-1}$. For both figures color represents laser number.

We have seen that random misalignment can cause perfect frequency locking and improve phase synchronization of an otherwise poorly synchronized diode laser array. Can engineered disorder achieve a similar effect? Apparently so: Figure 4 shows an example of phase synchronization in a 100-diode two-dimensional array subject to four different types of disorder. In each panel, the data represent 100 random realizations of disorder, all based on the same disordering principle. Linear and random disorder result in a high level of synchrony $\langle S \rangle$, while sinusoidal and constant disorder lead to rather poor synchrony. One could interpret the effect of certain types of spatial disorder as reducing spatial symmetries in the time-delay and therefore reducing the number of available states to the system (random and linear), while others (sinusoidal and constant disorder) conserve or only mildly reduce spatial symmetries in time-delays.

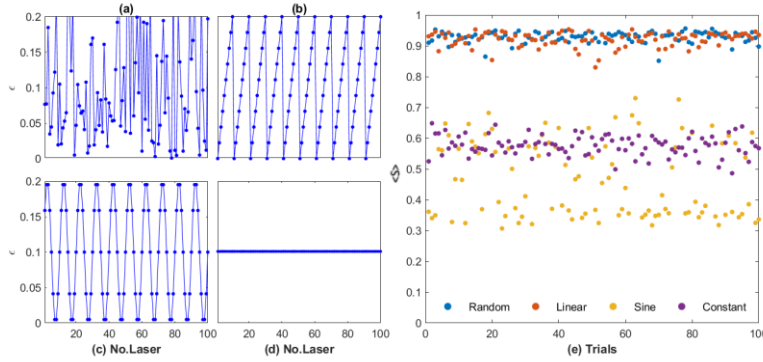


Figure 4: Right panel (e) shows synchrony level $\langle S \rangle$ for 100 realizations of disorder: (a) random normal distribution (b) linear, (c) sinusoidal and (d) constant. All disorders have average $\varepsilon = 0.1$. 100 diodes are arranged as a 10x10 array.

To summarize, we have demonstrated how one type of disorder can mitigate the destructive effect of another type. In this case, disorder in time-delay between laser elements seems to overcome the effects of heterogeneity. The reduced model for frequency-locking in the system suggests that the mechanism might be relevant in other types of systems and that the underlying mechanism adds to the list of other well-known mechanisms. We believe the results presented in this paper pose an important question about how disorder (random and/or engineered) can be used to overcome the effects of heterogeneity and improve frequency and phase-locking in large single-mode semiconductor diode arrays.

Acknowledgement: YB would like to acknowledge support from the Office of Naval Research.

References:

1. A. Pikovsky, M. Rosenblum and J. Kurths, Synchronization, Cambridge University Press, 2003.
2. J. A. Acebrón, L. L. Bonilla, C. J. P. Vicente, F. Ritort, and R. Spigler, Rev. Modern Phys. **77**, 137 (2005).
3. M. C. Soriano, et al., Rev. Modern Phys. **85**, 421 (2013).
4. L. M. Pecora and T. L. Carroll, Phys. Rev. Lett. **80**, 2109 (1998).
5. L. M. Pecora, F. Sorrentino, A. M. Hagerstrom, T. E. Murphy, and R. Roy, Nature Commun. **5**, 1 (2014).
6. D. Abrams and S. Strogatz, Phys. Rev. Lett. **93**, 174102 (2004).
7. T. Dahms, J. Lehnert and E. Schöll, Phys. Rev. E **86**, 16202 (2012).
8. F. Sorrentino, L. M. Pecora, A. M. Hagerstrom, T. E. Murphy, and R. Roy, Sci. Adv. **2** (4) (2016).
9. L. M. Pecora, and T. L. Carroll, Phys. Rev. Lett. **64**, 821 (1990).
10. J. D. Hart, K. Bansal, T. E. Murphy and R. Roy, Chaos **26**, 94801 (2016).
11. C. R. S. Williams, T. E. Murphy, R. Roy, F. Sorrentino, T. Dahms, and E. Schöll, Phys. Rev. Lett. **110**, 64104 (2013).
12. J. Shena, J. Hizanidis, P. Hövel, and G. P. Tsironis, Phys. Rev. E **96**, 3 (2017).
13. J. Shena, J. Hizanidis, V. Kovanis, and G. P. Tsironis, Sci. Rep. **7**, 1 (2017).
14. B. Liu, Y. Liu, and Y. Braiman, Opt. Express **18**, 7361 (2010).

15. B. Liu, and Y. Braiman, *Opt. Express* **21**, 31218 (2013).
16. T. Y. Fan, *IEEE J. Sel. Top. Quantum Electron.* **11**, 567 (2005).
17. E. Kapon, J. Katz, and A. Yariv, *Opt. Lett.* **9**, 125 (1984).
18. J. R. Leger, and G. Mowry, *Appl. Phys. Lett.* **63**, 2884 (1993).
19. B. Liu, and Y. Braiman, *Opt. Commun.* **414**, 202 (2018).
20. A. A. Ishaaya, N. Davidson, and A. A. Friesem, *IEEE J. Sel. Top. Quantum Electron.* **15**, 301 (2009).
21. C. J. Corcoran, and F. Durville, *Opt. Express* **22**, 8420 (2014).
22. G. Schimmel, I. Doyen, S. Janicot, M. Hanna, P. Georges, G. Lucas-Leclin, J. Decker, P. Crump, G. Erbert, S. Kaunga-Nyirenda, D. Moss, S. Bull, E. C. Larkins, U. White, and M. Taub, *Proc. of SPIE* **9733**, 97330I (2016).
23. R. Lang and K. Kobayashi, *IEEE J. Quantum Electron.* **16**, 347 (1980).
24. H. G. Winful, *Phys. Rev. A* **46**, 6093 (1992).
25. H. G. Winful and L. Rahman, *Phys. Rev. Lett.* **65**, 1990 (1990).
26. R.-D. Li and T. Erneux, *Phys. Rev. A* **46**, 4252 (1992).
27. B. Kim, N. Li, A. Locquet, and D. S. Citrin, *Opt. Express* **22**, 2348 (2014).
28. A. Argyris, M. Bourmpos and D. Syvridis, *Opt. Express* **24**, 5600 (2016).
29. R. L. Davidchack, Y.-C. Lai, A. Gavrielides and V. Kovanis, *Physica D* **145**, 130 (2000).
30. R. Benzi, A. Sutera, and A. Vulpiani, *J. Phys. A* **14**, (1981); C. Nicolis and G. Nicolis, *Tellus* **33**, 225 (1981).
31. L. Gammaitoni, P. Hanggi, P. Jung, and F. Marchesoni, *Rev. Modern Phys.* **70**, 223 (1998).
32. Z. G. Nicolaou, M. Sebek, I. Z. Kiss, and A. E. Motter, *Phys. Rev. Lett.* **125**, 094101 (2020).
33. Y. Braiman, J. F. Lindner, and W. L. Ditto, *Nature* **378**, 465 (1995).
34. A. Gavrielides, T. Kottos, V. Kovanis, and G. P. Tsironis, *Phys Rev E* **58**, 5529 (1998).
35. A. Valizadeh, M. R. Kolahchi, and J. P. Straley, *Phys. Rev. B* **82**, 144520 (2010).
36. P. S. Skardal and A. Arenas, *Phys. Rev. E* **89**, 062811 (2014).
37. H. Hong, K. P. O’Keeffe, and S. H. Strogatz, *Phys Rev. E* **93**, 022219 (2016).
38. S. F. Brandt, B. K. Dellen, and R. Wessel, *Phys. Rev. Lett.* **96**, 034104 (2006).
39. R. Chacon and P. J. Martinez, *Phys. Rev. Lett.* **98**, 224102 (2007).
40. Y. Braiman, W. L. Ditto, K. Wiesenfeld, and M. L. Spano, *Phys. Lett. A* **206**, 54 (1995).
41. Y. Zhang, J. L. Ocampo-Espindola, I. Z. Kiss, A. E. Motter, *PNAS*, **118**(21), e2024299118 (2021).
42. H. Bruesselbach, D. C. Jones, M. S. Mangir, M. Minden, and J. L. Rogers, *Optics Letters* **30**, 1339 (2005).
43. J. E. Rothenberg, *Proc. SPIE* 6873, *Fiber Lasers V: Technology, Systems, and Applications*, 687315 (2008).

44. E. Bochove and S. A. Shakir, IEEE Journal Selected Topics Quantum Electronics **15**, 320 (2009).
45. B. Abaie, M. Peysokhan, J. Zhao, E. Antonio- Lopez, R. Amezcua-Correa, A. Schülzgen, and A. Mafi, Optica **5**, 984 (2018).
46. S. Petkoski, A. Spiegler, T. Proix, P. Aram, J.-J. Temprado, and V. K. Jirsa Phys. Rev. E **94**, 012209 (2016).
47. W.-T. Yu, J. Tang, J. Ma, and X. Yang, Europhys. Lett. **114**, 50006 (2016).
48. K. Wiesenfeld, P. Colet, and S. H. Strogatz, Phys. Rev. Lett. **76**, 404 (1996).
49. R. Lang and K. Kobayashi, IEEE J. Quantum Electron. **16**, 347 (1980).
50. C. Masoller, IEEE J. Quantum Electron. **33**, (1997).
51. G. Agrawal, IEEE J. Quantum Electron. **23**, 860 (1987).
52. C. Masoller, IEEE J. Quantum Electron. **33**, 795 (1997).
53. C. H. Henry, IEEE J. Quantum Electron. **18**, 259 (1982).
54. M. Yousefi, D. Lenstra, and G. Vemuri, IEEE J. Sel. Top. Quantum Electron. **10**, 955 (2004).
55. M. Soriano, IEEE J. Quantum Electron. **47**, 368 (2011).
56. R. Toral, and P. Colet, *Stochastic Numerical Methods: An Introduction for Students and Scientists*. (Wiley, 2014).
57. K. Hirosawa, F. Shohda, T. Yanagisawa, and F. Kannari, Proc. SPIE **9342**, 934216 (2015).
58. N. Nair, E. Bochove, A. B. Aceves, M. R. Zunoubi, and Y. Braiman, Proceedings of SPIE **9343**, (2015).
59. D.-S. Seo, J.-D. Park, J. G. McInerney, and M. Osiński, IEEE J. Quantum Electron. **25**, 2229 (1989).
60. Xing-Guang Wang, Bin-Bin Zhao, Yu Deng, Vassilios Kovanis, and Cheng Wang, Phys. Rev. A **103**, 023528 (2021).
61. N. Nair, E. Bochove, and Y. Braiman, Opt. Comm. **430**, 104 (2019).
62. N. Nair, E. Bochove, and Y. Braiman, Opt. Exp. **26**, 20040 (2018).
63. V. Rottschäfer and B. Krauskopf, Int. J. Bifurc. Chaos **17**, 1575 (2007).
64. C. Masoller and N. B. Abraham, Phys. Rev. A. **57**, 1313 (1998).
65. B. Tromborg, J. Osmundsen and H. Olesen, IEEE J. Quantum Electron. **20**, 1023 (1984).
66. S. Yanchuk, and M. Wolfrum, J. Appl. Dyn. Syst. **9**, 519 (2010).
67. P. M. Alsing, V. Kovanis, A. Gavrielides, and T. Erneux, Phys. Rev. A. **53**, 4429–4434 (1996).
68. B. Kim, N. Li, D. Choi, A. Locquet, and D. S. Citrin, Proc. SPIE **9134**, 965 (2014).
69. J. Mørk, M. Semkow, and B. Tromborg, Electron. Lett. **26**, 609 (1990).
70. D. Lenstra, Opt. Commun. **81**, 209 (1991).
71. R. Vicente, J. Mulet, M. Sciamanna, and C. R. Mirasso, Proc. SPIE **5349**, (2004).
72. O. D’Huys, T. Jüngling, and W. Kinzel, *On the Interplay of Noise and Delay in Coupled Oscillators*, in *Control of Self-Organizing Nonlinear Systems. Understanding Complex Systems.*, edited by E. Schöll, S. Klapp, P. Hövel (Springer, Cham, 2016) pp. 127-145.

73. M. K. S. Yeung, and S. H. Strogatz Phys. Rev. Lett. **82**, 648 (1999).
74. A. I. Khibnik, Y. Braiman, T. A. B. Kennedy, K. Wiesenfeld, Physica D. **111**, 295 (1998).